VOLUME 80 SEPARATE No. 434

PROCEEDINGS

AMERICAN SOCIETY
OF
CIVIL ENGINEERS

APRIL, 1954

ANALYSIS AND TESTS OF A CYLINDRICAL SHELL ROOF MODEL

by Bruno Thurlimann and
Bruce G. Johnston, M. ASCE

STRUCTURAL DIVISION

{Discussion open until August 1, 1954}

Headquarters of the Society
33 W. 39th St.
New York 18, N. Y.

PRICE $0.50 PER COPY

This paper was published at 1745 S. State Street, Ann Arbor, Mich., by the American Society of Civil Engineers. Editorial and General Offices are at 33 West Thirty-ninth Street, New York 18, N. Y.

AMERICAN SOCIETY OF CIVIL ENGINEERS

Founded November 5, 1852

PAPERS

ANALYSIS AND TESTS OF A CYLINDRICAL SHELL ROOF MODEL

BY BRUNO THÜRLIMANN[1] AND BRUCE G. JOHNSTON,[2] M. ASCE

[1] Research Asst. Prof., Fritz Eng. Lab., Lehigh Univ., Bethlehem, Pa.

[2] Prof. of Structural Eng., Civ. Eng. Dept., Univ. of Michigan, Ann Arbor, Mich.; formerly Director of Fritz Eng. Lab., Lehigh Univ., Bethlehem, Pa.

SYNOPSIS

Analytical expressions for the effective width of cylindrical shells are presented herein. These formulas are used for the analysis of a cylindrical shell roof acted upon by horizontal longitudinal forces. Also studied are the influences of foundation movements, temperature changes, and shrinkage.

A comparison is made between theoretical results and experimental measurements obtained from a model of an actual cylindrical shell roof constructed in the approximate ratio of 1 to 30. It is established that there is satisfactory agreement between the theoretical analysis and the test results.

INTRODUCTION

It is a common misconception that the use of shells as structural elements is a development of the twentieth century. Two thousand years before, the Romans had constructed the Pantheon, which was covered by a spherical shell with a diameter of approximately 145 ft. The cupolas of the cathedral in Florence (Italy) and St. Peter's Basilica in Rome (Italy), built during the fifteenth and sixteenth centuries, respectively, and having a diameter of approximately 140 ft, are examples of remarkable craftmanship, based only on experience and intuition. The contribution of the twentieth century to this type of construction consists in the development of a rational analysis which can be used to predict the state of stress in the shell.

The development of the shell theory was initiated by A. E. H. Love (1)[3]

[3] Numerals in parentheses, thus (1), refer to corresponding items in the Bibliography (see Appendix II).

who derived the differential equations for curved plates. E. Meissner (2) (3) succeeded in integrating these equations for spherical and conical shells. F. Bauersfeld (4), U. Finsterwalder (5), and F. Dischinger (6) made possible the

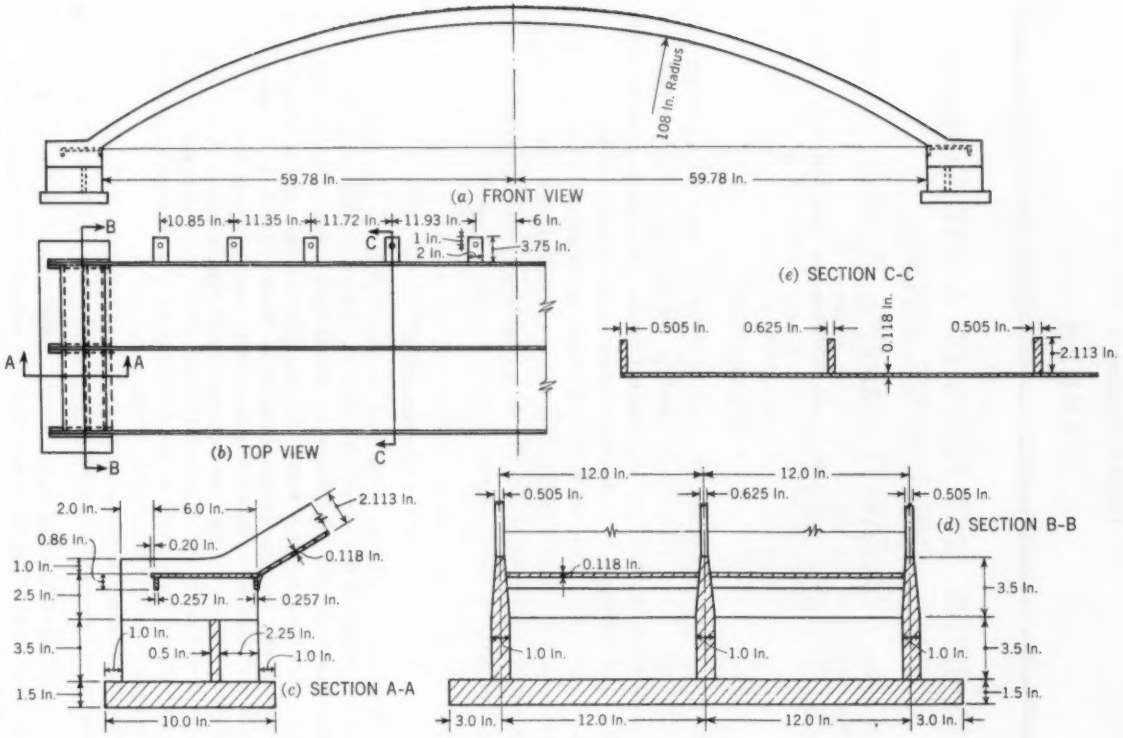

FIG. 1.—SHELL ROOF MODEL

application of the theory to the analysis of actual structures. A number of reinforced concrete shells were built in Europe immediately following World War I, and there were concurrent theoretical contributions.

The arena in Hershey, Pa., built in 1936 (7), was the first modern cylindrical shell roof constructed in the United States. In the years that followed, and especially during and subsequent to World War II, a number of shell roofs were built—to be used as storage houses, factory buildings, airplane hangars, sport arenas, and armories—covering a total of 10,000,000 sq ft.

At present (1953) the largest span for a cylindrical shell roof is 340 ft (the hangars at Rapid City, S. Dak. (8) and at Limestone, Me. (9)). These large-span structures accentuated certain problems which were of secondary importance in the previously built smaller structures. Because there is a tendency toward increasing the span of shell structures, a careful analysis of the pertinent problems is mandatory.

The supporting ribs in cylindrical shell roofs can be designed as T-sections to include the additional effective section provided by the shell. A study (10) of the interaction between the ribs and shell shows that an "effective width" of the shell can be determined and the combined section used in a relatively simple arch analysis of the rib structure.

Lateral horizontal forces, caused by wind action on the front and back doors of large-span cylindrical shell roofs, can reach a considerable magnitude. The influence of these forces on the structure cannot be considered secondary. A difference of temperature inside and outside the building can produce relatively high thermal stresses. Shrinkage and plastic flow greatly affect the stability of the structure. These are a few of the problems to be considered in the analysis of large shell roofs.

During the period from January 1, 1949, to February 15, 1951, a research program on shell arch roofs was conducted at the Fritz Engineering Laboratory of Lehigh University at Bethlehem, Pa., with special emphasis on the previously cited problems. A careful theoretical study of the problems was made, and the results were checked experimentally on the model of a cylindrical shell roof shown in Fig. 1. This paper presents three contributions to the analysis of shell roofs made during the course of the research program. It will be shown that the model tests were in excellent agreement with the theory.

Effective Width of Cylindrical Shells

The stress distribution in the flange of a T-beam with a straight axis, subjected to bending in the plane of the rib, is not constant over the width of the flange. This condition is shown in Fig. 2. Simple beam theory, based on the Navier-Bernoulli hypothesis (a plane cross section remains plane after bending) can be utilized if the actual width of the flange is replaced by the effective width b. T. von Kármàn, Hon. M. ASCE (11), was the first investigator to derive the correct theoretical expression for this effective width (12). Shear lag is responsible for the considerable damping of the direct stresses in the flange in the direction of the rib.

In Fig. 3 there is shown a cylindrical shell stiffened by a rib in the circumferential direction. Arbitrary loads, acting in the plane of the rib, will cause direct forces N_ϕ per unit width in the circumferential direction. The actual

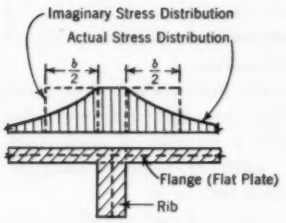

FIG. 2.—T-BEAM

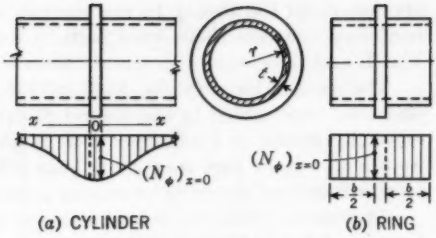

FIG. 3.—CYLINDRICAL SHELL

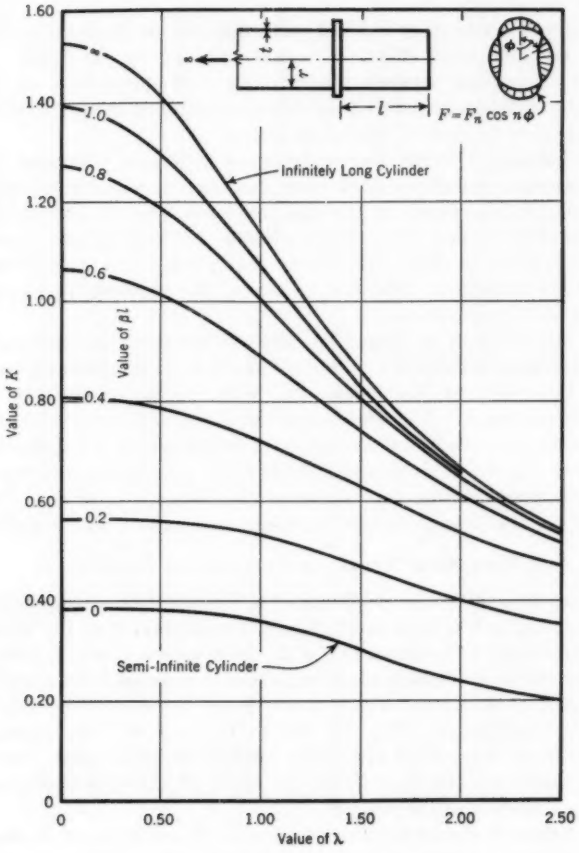

FIG. 4.—THE RELATION AMONG K, λ, AND β

cylinder can be replaced by a ring of width b for which a constant direct force $(N_\phi)_{x=0}$ (equal to $(N_\phi)_{x=0}$ for the cylinder) over the entire width is assumed. By determining the width b so that

$$\left[b(N_\phi)_{x=0}\right]_{\text{Ring}} = \left[\int N_\phi \, dx\right]_{\text{Cylinder}} \quad \ldots\ldots\ldots\ldots\ldots\ldots (1)$$

the stresses in the ribs are obviously identical for both structures under an equal load system. If width b is known, determination of the rib stresses becomes a problem that can be solved by the use of the simple beam theory.

Analytical expressions for the effective width, based on the general bending theory of cylindrical shells (13), have been derived by one of the writers (14). There is also a short report on this study in which the analytical values for b are compared with experimental results (10).

C. B. Biezeno and J. J. Koch (15) have derived expressions for the effective width of a shell that extends indefinitely on either side of a rib. This is a special case ($\beta l = \infty$ in Fig. 4) of the general solution in which the rib can be any distance l from a free boundary. It is shown that, essentially, two effects govern the effective width of cylindrical shells: (*a*) The lag of the direct shear forces in the plane of the shell (as in the case of a T-beam with a straight axis) and (*b*) the radial escaping of the shell under the circumferential direct forces N_ϕ. In general, b can be written (14) as

$$b = K\sqrt{r\,t} \quad \ldots\ldots\ldots\ldots\ldots\ldots\ldots\ldots\ldots (2)$$

in which r is the radius of the cylinder, t denotes the thickness of the cylinder, and K equals $f(\lambda, \beta l)$ (Fig. 4).

The parameter λ (Fig. 4) takes into account the influence of the direct shear forces on the effective width

$$\lambda = n\sqrt{\frac{t}{r}} \quad \ldots\ldots\ldots\ldots\ldots\ldots\ldots\ldots\ldots (3)$$

in which n depends on the variation of the stresses in circumferential direction and is the number of complete waves made by a harmonic function around the circumference of the cylinder (Fig. 4). For n equal to zero, the stress distribution has axial symmetry, and the effective width has its maximum value. The parameter $\beta\, l$ is dependent on the length of the overhang of the shell l and on the shell constant (13*a*)

$$\beta = \frac{\sqrt[4]{3}}{\sqrt{r\,t}} \quad \ldots\ldots\ldots\ldots\ldots\ldots\ldots\ldots\ldots (4)$$

As shown in Fig. 4, the shell is assumed to extend infinitely on the left side. This can be assumed safely if the product $\beta\, s$ exceeds 2.4, in which s is the distance of the left end from the rib (14*a*).

Taking the effective width b as the flange and the rib as the web of a T-section, the Bernoulli-Navier hypothesis leads to the correct values for the rib stresses. Also, denoting the circumferential stress along the connecting line of rib and shell by σ_a, the total direct force F in the shell is the integral of all

direct forces ($N_\phi = \sigma_\phi\, t$) over the entire length of the shell or is equal to the product of the stress σ_a, the thickness t, and the effective width b. Thus,

$$F = \int N_\phi\, dx = \sigma_a\, t\, b \qquad (5)$$

For a given value of F and a given set of boundary conditions, all forces and moments in the shell can be determined. Tables and graphs which reduce these computations to a minimum are available (14).

Knowledge of the effective width of a cylindrical shell simplifies an involved problem of elasticity to a common problem of the ordinary beam theory. This effective width will be used subsequently in the analysis of shell roofs.

The Effect of Horizontal Longitudinal Forces

The action of the wind on the front and back doors of cylindrical shell roofs produces considerable horizontal forces. This type of loading will be analyzed, and numerical results will then be compared to test results obtained on a model.

During construction, the roof is erected in units in order to re-use the forms and to provide expansion joints. One unit of a cylindrical shell roof is shown in Fig. 5 and it is subjected to horizontal forces in the direction of the axis. On a cross section a shear force V, a bending moment M_B, and a twisting moment M_T are acting. It is necessary to find the stress distribution resulting from these forces and moments.

In Fig. 6 there is shown a part of a cylindrical shell of infinitesimal width $r\, d\phi$. The forces and moments acting on the shell element are defined in Fig. 7. The direct force N_x in the axial direction is equal to the applied uniformly distributed load p at the rib $x = 2\,l$. The force N_x equals zero at the rib $x = 0$. Assuming a linear variation of N_x along the x-axis, then

$$N_x = \frac{x\, p}{2\, l} \qquad (6a)$$

and

$$\frac{\partial N_x}{\partial x} = \frac{p}{2\, l} \qquad (6b)$$

The assumption of a linear variation of N_x is especially true for shell roofs whose width is relatively small in comparison to the span L. The equilibrium of an infinitesimal shell element $dx\, r\, d\phi$ in the x-direction results in (Fig. 6)

$$\frac{\partial N_x}{\partial x}\, dx\, r\, d\phi + \frac{\partial N_{\phi x}}{\partial \phi}\, d\phi\, dx = 0 \qquad (7a)$$

Replacing $\partial N_x/\partial x$ by its value from Eq. 6*b* results in

$$\frac{\partial N_{\phi x}}{\partial \phi} = -\frac{r\, p}{2\, l} \qquad (7b)$$

By integrating Eq. 7*b* and considering the fact that the shear force $N_{x\phi}$ is zero at the center of the span, because of symmetry, $N_{\phi x}$ becomes

$$N_{\phi x} = -\frac{r\, p\, \phi}{2\, l} \qquad (8)$$

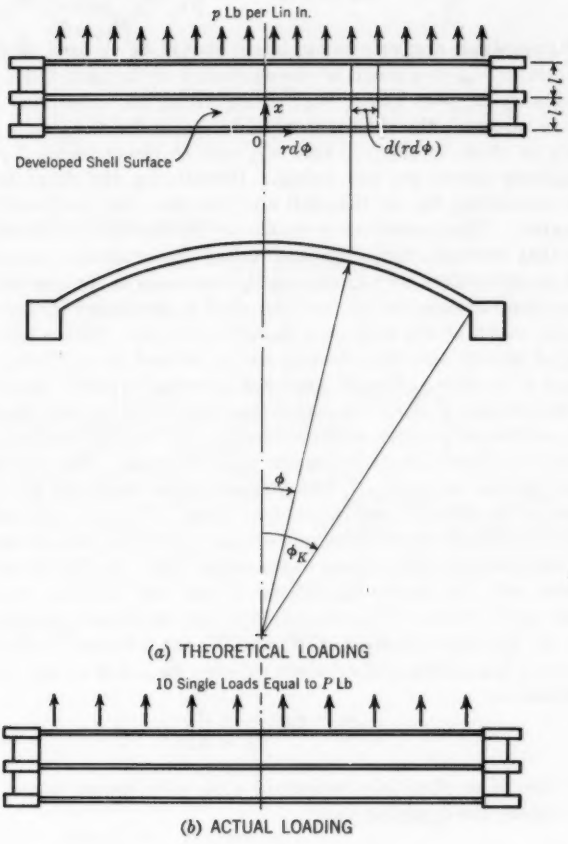

FIG. 5.—ONE UNIT OF A CYLINDRICAL SHELL ROOF

It follows that $N_{\phi x}$ is constant for a section in which ϕ is a constant and varies in proportion to the angle ϕ along the span of the shell. From the equality of the shearing stresses ($\tau_{\phi x} = \tau_{x\phi}$) the direct shear forces, $N_{x\phi}$, in a radial direction can be considered equal to the direct shear forces $N_{\phi x}$. Thus,

$$N_{x\phi} \cong N_{\phi x} = -\frac{r\,p\,\phi}{2\,l} \quad \ldots\ldots\ldots\ldots\ldots\ldots\ldots\ldots (9)$$

Eq. 9 is a reasonable approximation, but it should be realized that $N_{x\phi}$ is not exactly equal to $N_{\phi x}$ as a result of the curvature of the shell (16).

If imaginary support forces $N_{x\phi}$, acting along the outer ribs ($x = 0$ and $x = 2\,l$) are assumed, the shell is in equilibrium under the load p and is subjected only to shear forces $N_{x\phi}$ and $N_{\phi x}$ and to direct forces N_x. Actually these imaginary forces are not acting. Introducing the shear forces $-N_{x\phi}$ along the connecting line of the shell and the ribs, the imaginary forces $N_{x\phi}$ are eliminated. This procedure is similar to the method of moment distribution. In that method, the joints are locked by imaginary moments which afterward are eliminated by introducing the moments in the opposite direction. The interaction between the rib and the shell is accounted for by considering the effective width of the shell as a flange of the rib. This effective section, consisting of the rib and the effective width, is used in analyzing the arches.

Analysis of the Ribs.—The rib at $x = 2\,l$ is acted upon by shear loads, $N_{x\phi}$, per unit length, acting along the connecting line of the rib and the shell. The loads are considered positive as shown in Fig. 8. On the rib x equal to zero, the positive $N_{x\phi}$-forces are acting in the opposite sense. Fig. 6 shows the sign convention for the forces $N_{x\phi}$. The distance from the loads $N_{x\phi}$ to the centroidal axis of the effective section is equal to z_a. The rib is an elastically restrained arch, having only two redundants as a result of the symmetry of the structure and the load with respect to the center line. In Fig. 8 one half of one rib is shown with the horizontal thrust H_c and the bending moment M_c as redundants at the center. The two geometrical conditions furnishing the two equations for the determination of H_c and M_c are a known horizontal movement δ_K of the foundation and a known rotation θ_K. For a fully restrained rib the conditions are

$$\left.\begin{aligned} \phi = \phi_K : \delta_K &= 0 \\ \theta_K &= 0 \end{aligned}\right\} \quad \ldots\ldots\ldots\ldots\ldots\ldots\ldots\ldots (10)$$

In the case of an elastically restrained arch, with known measured foundation movements, the conditions are

and

$$\left.\begin{aligned} \phi = \phi_K : \delta_K &= (\delta_K)_{meas} \\ \theta_K &= (\theta_K)_{meas} - \kappa\, M_K \end{aligned}\right\} \quad \ldots\ldots\ldots\ldots\ldots\ldots\ldots\ldots (11)$$

The terms $(\delta_K)_{meas}$ and $(\theta_K)_{meas}$ are the measured horizontal displacement and rotation of the abutment, respectively. The symbol κ is the coefficient of elastic restraint, and the product $-\kappa\, M_K$, in which M_K is the restraining moment, represents the elastic end rotation of the rib.

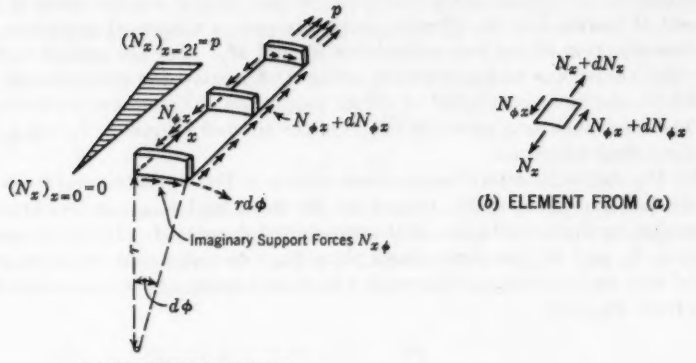

FIG. 6.—PART OF A SHELL ROOF

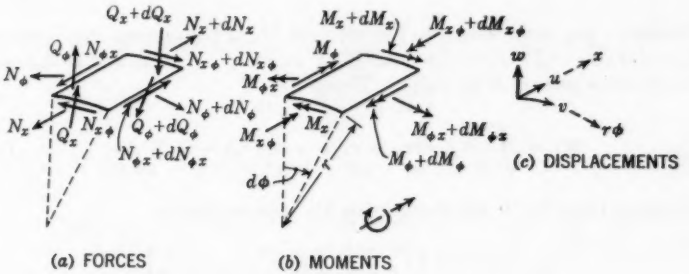

FIG. 7.—FORCES AND MOMENTS ACTING ON THE SHELL ELEMENT

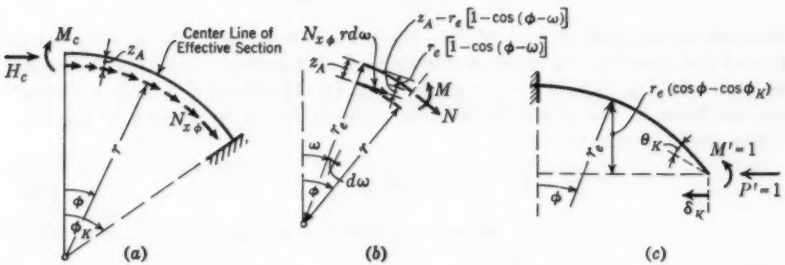

FIG. 8.—SHEAR LOADS UPON THE ROOF SHELL

In general, the shape of the center line of the rib and the variation of the moment of inertia I of the effective section require a numerical procedure for the determination of the two redundants H_c and M_c. For the special case of a circular center line and a constant moment of inertia, the computation for H_c and M_c can be accomplished by direct integration. Extension can be made to other cases such as a parabolic shape of the rib and I equal to $I_c/\cos\phi$, or to a numerical solution.

For the statically determinate system shown in Fig. 8, the normal force N_o and the bending moment M_o, caused by the shear load $N_{x\phi}$, can be obtained by integrating the contribution of the distributed shear load. If ϕ is the angle at which N_o and M_o are determined, then $N_{x\phi}\, r\, d\omega$ represents the shear load applied over an infinitesimal rib length $r\, d\omega$ at any angle ω between zero and ϕ. Then from Fig. 8(*b*),

$$N_o = -\int_o^{\phi} N_{x\phi}\, r \cos(\phi - \omega)\, d\omega \qquad (12a)$$

Substituting from Eq. 9 and integrating Eq. 12*a* results in

$$N_o = -\frac{r^2 p}{2 l}(1 - \cos\phi) \qquad (12b)$$

Similarly, the contribution to the moment M_o of the incremental shear load is $N_{x\phi}\, r\, d\omega\{Z_a - r_c[1 - \cos(\phi - \omega)]\}$, in which $r_c = r + z_a$ and is the radius of the effective section (Fig. 8(*b*)). Therefore,

$$M_o = \int_o^{\phi} N_{x\phi}\, r\{z_a - r_c[1 - \cos(\phi - \omega)]\}\, d\omega \qquad (13a)$$

Substituting from Eq. 9 and integrating Eq. 13*a* results in

$$M_o = \frac{r^2 r_c\, p}{2 l}\left[\left(1 - \frac{z_a}{r_c}\right)\frac{\phi^2}{2} - 1 + \cos\phi\right] \qquad (13b)$$

The total normal force N and the total bending moment M are (Fig. 8(*a*))

$$N = N_o - H_c \cos\phi \qquad (14)$$

and

$$M = M_o + H_c\, r_c\,(1 - \cos\phi) + M_c \qquad (15)$$

In order to compute H_c and M_c, the horizontal displacement δ_K and the rotation of the abutment θ_K must be determined. Choosing a virtual load system as shown in Fig. 8(*c*), P' equal to unity at the abutment produces a virtual normal force N' and a virtual bending moment M' at an angle ϕ in the rib. These qualities are related by

$$P' = 1: \quad N' = -\cos\phi \qquad (16)$$

$$M' = -r_c(\cos\phi - \cos\phi_K) \qquad (17)$$

By use of the work equation, the displacement δ_K of the actual system is expressed as the work done by the virtual load ($P' = 1$):

$$\delta_K = \int \frac{M'\,M\,ds}{E\,I} + \int \frac{N'\,N\,ds}{E\,A} \quad \ldots\ldots\ldots\ldots\ldots\ldots (18a)$$

in which

$$ds = r_c\,d\phi \quad \ldots\ldots\ldots\ldots\ldots\ldots\ldots\ldots\ldots (18b)$$

and A is the cross-sectional area. The influence of the normal force N on the displacement is extremely small and therefore can be safely disregarded. Assuming that the product $E\,I$ is a constant and replacing M' and M by their values from Eqs. 17 and 15, respectively, Eq. 18a becomes

$$\delta_K = \frac{1}{E\,I}\int_o^{\phi_K} [-r_c\,(\cos\phi - \cos\phi_K)] \times [M_o + H_c\,r_c\,(1 - \cos\phi) + M_c]\,r_c\,d\phi \ldots (19)$$

Replacing M_o by its value from Eq. 13b and integrating Eq. 19,

$$-\delta_K\frac{E\,I}{r_c^2} = M_c\,(\sin\phi_K - \phi_K\cos\phi_K) + H_c\,r_c\,(\sin\phi_K + \tfrac{1}{4}\sin 2\,\phi_K - \tfrac{1}{2}\,\phi_K - \phi_K\cos\phi_K) + \frac{r^2\,p}{2\,l}\,r_c\left\{\left(1 - \frac{z_a}{r_c}\right)\left[\phi_K\cos\phi_K + \left(\frac{\phi^2_K}{2} - 1\right)\sin\phi_K - \frac{\phi^3_K}{b}\cos\phi_K\right] - \sin\phi_K - \tfrac{1}{4}\sin 2\,\phi_K + \tfrac{1}{2}\,\phi_K + \phi_K\cos\phi_K\right\} \ldots\ldots\ldots\ldots (20)$$

The rotation θ_K of the abutment is determined by the same procedure. The virtual moment M'_K equal to unity of Fig. 8(c) produces a bending moment M' equal to unity for any angle ϕ such that

$$M'_K = 1\colon\ M' = 1 \quad \ldots\ldots\ldots\ldots\ldots\ldots\ldots\ldots (21)$$

Inserting Eqs. 21 and 15 into the work equation,

$$\theta_K = \int \frac{M'\,M\,ds}{E\,I} \quad \ldots\ldots\ldots\ldots\ldots\ldots\ldots\ldots (22)$$

results in

$$\theta_K = \frac{1}{E\,I}\int_o^{\phi_K} [M_o + H_c\,r_c\,(1 - \cos\phi) + M_c]\,r_c\,d\phi \ldots\ldots (23)$$

If M_o is substituted by its value from Eq. 13b, the integration of Eq. 23 leads to

$$\theta_K\frac{E\,I}{r_c} = M_c\,\phi_K + H_c\,r_c\,(\phi_K - \sin\phi_K) + \frac{r^2}{2\,l}\frac{p}{}\,r_c\left[\left(1 - \frac{z_a}{r}\right)\frac{\phi^3_K}{6} - \phi_K + \sin\phi_K\right] \ldots (24)$$

Eqs. 20 and 24 each have the two unknowns, H_c and M_c. The normal force N and the bending moment M for any angle ϕ are determined from Eqs. 14 and 15 following the solution for the redundants. The stresses in the ribs are determined from

$$\sigma = \frac{N}{A} \pm \frac{M z}{I} \quad \ldots\ldots\ldots\ldots\ldots\ldots\ldots\ldots (25)$$

in which A and I are, respectively, the cross-sectional area and the moment of inertia of the effective section, consisting of the rib as a web and the effective width of the shell as a flange. The symbol z represents the distance of a fiber from the centroidal axis of the effective section.

Coefficient of Elastic Restraint.—In Eq. 11 a coefficient of elastic restraint κ was introduced. In arch bridges this coefficient provides for the elasticity of the soil and the abutment. In general, the arch cannot be considered fully restrained at the springing line.

During the tests performed on the model shown in Fig. 1 another consideration led to the introduction of κ. The section A–A in Fig. 1 gives a typical construction detail at the springing line of the rib and the shell. The latter is supported by a relatively flexible edge member. The rib, however, terminates in a very heavy end wall and can be regarded to be fully restrained. There are two extreme cases that can be considered: (1) The shell is held rigidly along the edge member and (2) the shell has a free edge. In the first case the N_ϕ-forces of the shell will be resisted by the support, and the effective width is sensibly constant down to the edge member as in Fig. 9(*a*). If there is no support at all, the effective width must be reduced to zero at the springing line as in Fig. 9(*b*). The actual condition lies between these two cases. Since this disturbance of the effective width of the shell has only a local effect, the reduction of the moment of inertia of the effective section can be accounted for by considering the value of I as being constant to the springing line and by assuming an elastic restraint for the rib. The higher flexibility of the effective section in the end zone is therefore concentrated at the springing line.

It is obvious that the magnitude of the coefficient of elastic restraint depends on the effectiveness of the edge member in supporting the shell. No theoretical analysis was made of κ during the investigations.

Determination of the Shell Forces.—The stress along the connecting line of the rib and shell σ_a is computed by use of Eq. 25, following the determination of the normal force N and the bending moment M of the effective section. The total circumferential direct force F of the shell is given by Eq. 5.

The problem consists of finding the forces and moments in the shell for a given F and a given set of boundary conditions. In the present case the boundary conditions for the shell at the ribs $x = 0$ and $x = 2\,l$ are

$$M_x = 0 \quad \ldots\ldots\ldots\ldots\ldots\ldots\ldots\ldots (26)$$

in which M_x is the bending moment of the shell in the axial direction. The condition given in Eq. 26 presupposes the neglect of the torsional stiffness of the rib. The influence of the middle rib on the stress distribution can be disregarded, the forces and moments being rapidly damped with increasing distance from the end ribs. The actual computations for these forces and moments are readily made by use of tables (14).

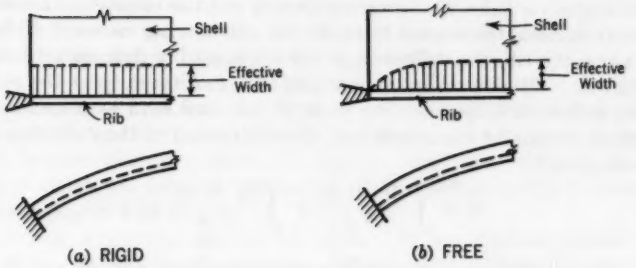

FIG. 9.—EXTREME CONDITIONS OF SHELL SUPPORT

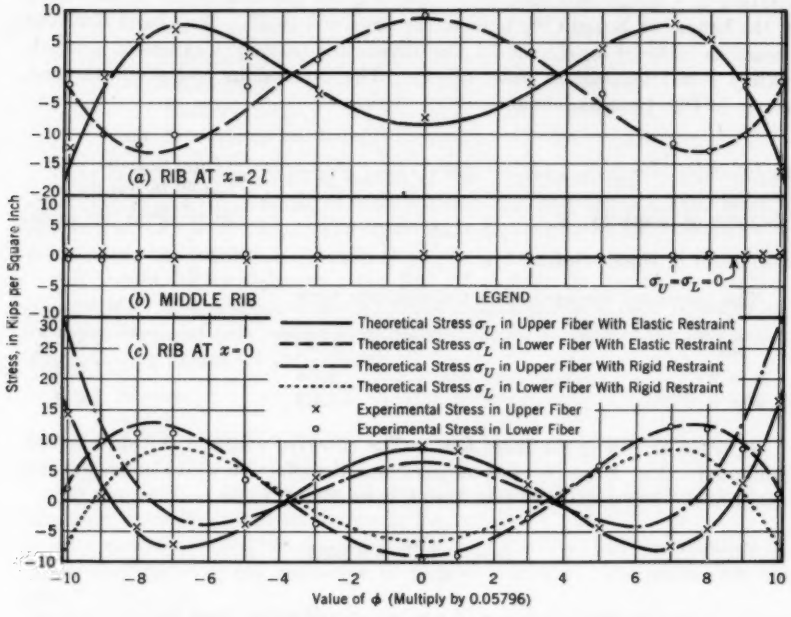

FIG. 10.—FIBER STRESSES IN THE RIBS WHEN THE MODEL IS SUBJECTED TO TEN LOADS OF 1,687.5 LB EACH ON THE EDGE AT $\bar{x} = 21$

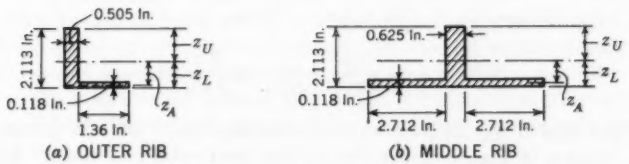

FIG. 11.—EFFECTIVE SECTION OF THE RIBS

Deflections of the Rib.—Knowing the area A and the moment of inertia I of the effective section, the normal force N, and the bending moment M for any angle ϕ along the rib, the deflection of the rib is readily determined from the work equation. Placing an imaginary load P' equal to unity at the point at which the deflection is desired, the work of this unit load as a result of the deformations caused by the actual load system is equal to the deflection under consideration, or

$$\delta = \int \frac{M' M \, ds}{E I} + \int \frac{N' N \, ds}{E A} \quad \ldots\ldots\ldots\ldots\ldots\ldots (27)$$

in which N' and M' are caused by the imaginary load, and M and N are a result of the actual loads.

Numerical Example.—The foregoing theory will be applied to the analytical solution of a model of a shell roof. Fig. 1 gives the dimensions of the model of the hangar at Rapid City built to the scale of 1 to 30. Structural steel was chosen as material for the model, the dimensions (a shell thickness of approximately $\frac{1}{8}$ in.) leaving no other choice. The dimensions and properties not shown in Fig. 1 are as follows:

Item	Value
ϕ_K for outer ribs	0.5866 radian
Load, p	140.62 lb per lin in.
Modulus of elasticity, E	30×10^6 lb per sq in.
Coefficient of elastic restraint, κ	$0.2 \frac{r_e}{E I}$

The measured movements of the supports were

Rib	δ_K, in inches $\times 10^2$	ϕ_K, in radians $\times 10^3$
$x = 2\,l$	1.03	−1.074
$x = 0$	−1.03	1.074

Effective Section of the Outer Ribs.—The effective width of the shell is first computed. Fig. 4 can be used to determine the effective width under general conditions. The coefficient β is found, from Eq. 4, to be

$$\beta = \frac{1.3161}{\sqrt{r\,t}} = 0.3687 \quad \ldots\ldots\ldots\ldots\ldots\ldots (28)$$

To determine the number n, the stress distribution along the rib in a circumferential direction must be known. Anticipating the final results, Fig. 10 shows the stresses in the ribs. The stress σ_L (σ_a has the same variation) in the lower fiber has approximately the form of a cosine function, with a half-wave length of from 0.35 radian to 0.40 radian. Thus,

$$n = \frac{\pi}{\text{half-wave length}} \cong \frac{3\,\pi}{2\,\phi_K} \quad \ldots\ldots\ldots\ldots\ldots\ldots (29)$$

The right side of Eq. 29 is an approximate expression for n in terms of the angle ϕ_K (shown in Fig. 8) and holds for this particular case only. Another

load would produce another variation of the stress σ_L. Substituting the numerical value for ϕ_K into Eq. 29 results in n equal to 8.03. The coefficient λ is found, from Eq. 3, to equal 0.26.

The two outer ribs have no overhang, and the distance to the middle rib can be considered to be infinite. Entering the chart in Fig. 4 with the values of βl equal to zero and λ equal to 0.26, the coefficient K is found to equal 0.38. It can be seen that for values of λ less than 0.75 the coefficient K and the effective width are sensibly constant. The effective width b, from Eq. 2, becomes equal to 1.36 in.

The area A and the moment of inertia I of the effective section are then computed. In Fig. 11 (*a*) there is shown the pertinent information for the outer rib. Further data for the outer rib are listed:

Item	Value
Area, A	1.227 sq in.
Distance, z_u	1.186 in.
Distance, z_L	0.926 in.
Distance, z_a	0.867 in.
Radius, r_c	108.926 in.
Moment of inertia, I	0.536 in.^{4}

The ratio of the moment of inertia of the effective section to the moment of inertia of the rib is equal to 1.35. Thus, the shell increases the bending stiffness of the rib by 35%. The shear loads $N_{x\phi}$ acting on the ribs are determined from Eq. 9.

All values are available to solve Eqs. 20 and 24 for the two redundants H_c and M_c. The solution is made for the assumption of a rigid restraint and an elastic restraint with measured displacement and rotation of the foundation. The following values are determined:

Restraint	H_c, in pounds	M_c, in inch-pounds
Rigid	−1,068	+3,156
Elastic	−1,457	+4,371

On the basis of these values of the redundants, the direct stresses in the ribs were determined and are shown in Fig. 10.

The computation of the direct forces N_ϕ and the cross bending moment M_x in the shell followed the procedure previously outlined. The results are presented in Fig. 12.

Experimental Investigation and Comparison.—An extensive experimental study on the model shown in Figs. 1 and 13 was made. Strains were recorded by 44 rosette (type AR-1), 137 cross (type AX-5), and 81 single (type A-5) SR-4 electrical strain gages. Displacements were measured by 20 Ames dial gages (with an accuracy of 0.001 in.), and the rotations were checked by two level bars (with an accuracy of 0.0002 radian). The actual loading consisted of ten equally spaced horizontal single loads as shown in Fig. 5(*b*). By virtue of St. Venant's principle the differences between the theoretical loading (assumed to be uniformly distributed) and the actual loading can cause only local differences in behavior.

The stresses in the ribs computed from the strain-gage readings are shown

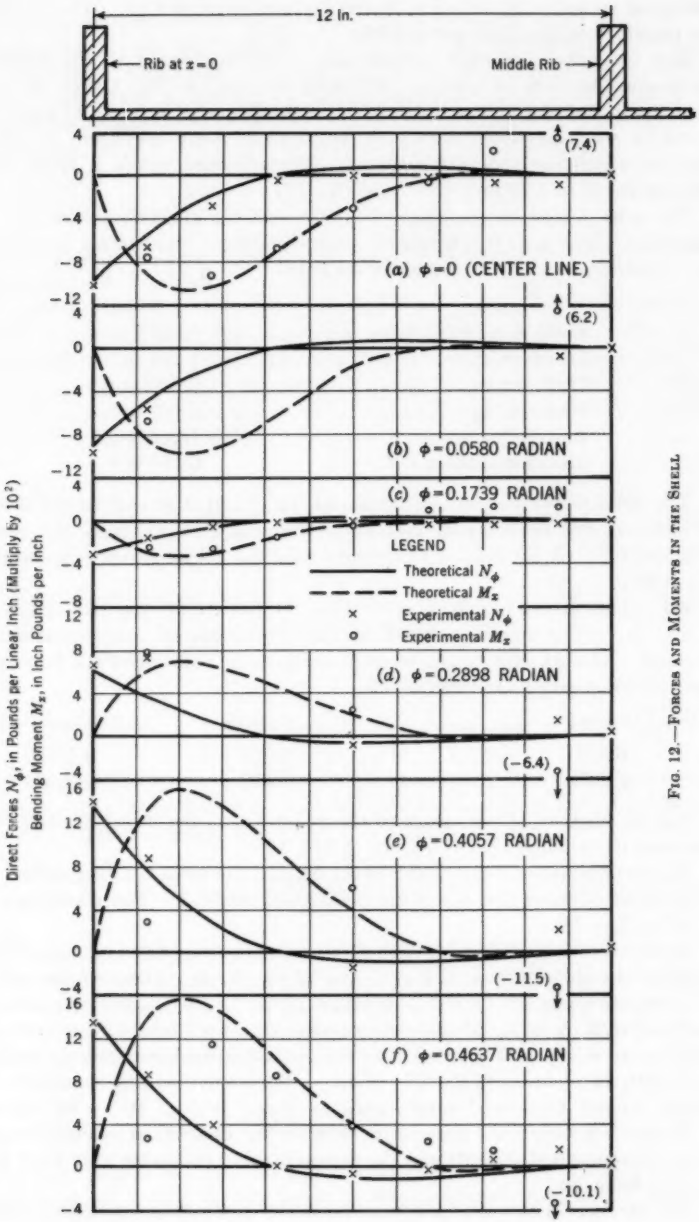

FIG. 12.—FORCES AND MOMENTS IN THE SHELL

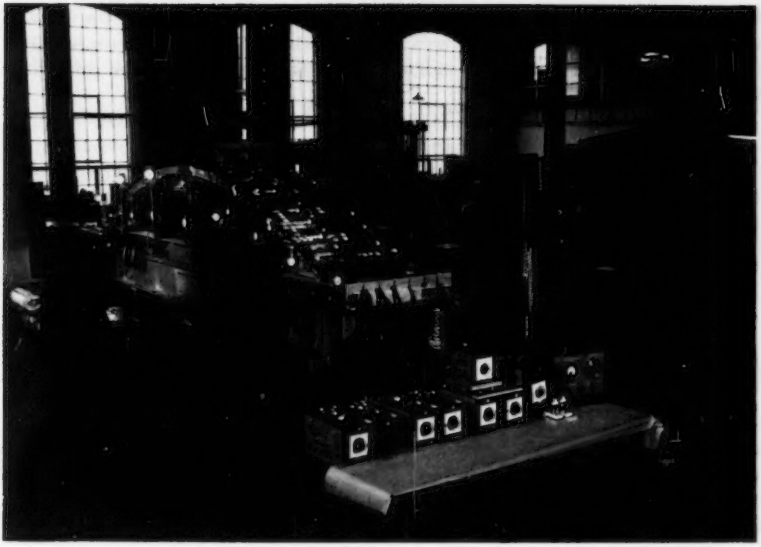

FIG. 13.—ROOF SHELL IN THE LABORATORY

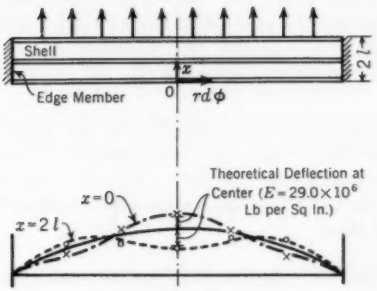

FIG. 14.—EXPERIMENTAL VERTICAL DEFLECTIONS OF THE OUTER RIBS FOR LATERAL LOADS

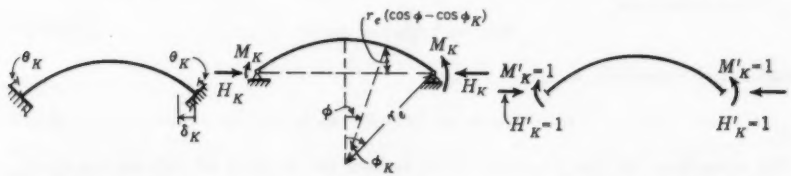

(a) ACTUAL SYSTEM (b) BASE SYSTEM (c) VIRTUAL LOAD SYSTEM

FIG. 15.—LOADS ON THE RIB

in Fig. 10. There is good agreement between the test results and the theoretical analysis if the analysis is made with an allowance for the elastic restraint of the rib. The introduction of κ is fully justified. In Fig. 12 the experimental N_ϕ (the direct force per unit width of the shell in the circumferential direction) and M_x (the bending moment per unit width in the axial direction) of the shell are plotted.

The agreement between the analytical and the theoretical results is quite close. It is of interest to note that the stress distribution is perfectly antisymmetric with respect to the middle rib. The middle rib is unstressed and therefore does not add to the strength of the structure under the present loading condition. The rib at x equal to $2\,l$ has exactly the opposite stresses of the rib at x equal to zero. This fact is also demonstrated in Fig. 14 in which the measured vertical deflections of both outer ribs are plotted.

Conclusions Concerning Horizontal Longitudinal Forces.—

1. The analysis of the effect of horizontal lateral wind loads on cylindrical shell roofs was fully confirmed by the experimental investigations on the model.

2. For actual shell roofs of the type constructed at Rapid City, the wind pressure on the front door (as prescribed by building codes) is from 30 lb per sq ft to 35 lb per sq ft, or approximately 1000 lb per lin ft of the rib. This results in maximum rib stresses of approximately 400 lb per sq in. Obviously, a stress of this magnitude cannot be considered a secondary one. By combining a number of shell units, these stresses can be lowered considerably.

Foundation Movements

The horizontal thrust of long-span shell roofs are of sufficient magnitude to offer serious foundation problems. In certain cases, tension ties have been found necessary to balance the horizontal thrust acting on the abutments (8*a*). It is usually impossible to prevent any foundation movements, except by special devices such as artificially stressing the tension ties between the abutments.

The general procedure for the computation of the forces in arches subjected to foundation movements can be used if the interaction, occurring between the ribs and the shell, is taken into account. This will be done by taking as a cross section of the rib the effective cross section formed by the rib and the effective width of the shell.

Analysis of the Ribs.—The horizontal displacement δ_K and the symmetrical rotations θ_K of the two abutments are considered. Unequal rotations θ_{Kl} and θ_{Kr} of the left and the right abutments can be solved by superimposing symmetrical rotations,

$$\theta_{K1} = \tfrac{1}{2}\,(\theta_{Kl} + \theta_{Kr}) \qquad (30)$$

and antisymmetrical rotations,

$$\theta_{K2} = \pm\,\tfrac{1}{2}\,(\theta_{Kl} - \theta_{Kr}) \qquad (31)$$

The advantage of this procedure is to reduce the number of redundants from three to two.

The rib, shown in Fig. 15(*a*), has two redundants—the horizontal thrust

H_K and the end moment M_K. Introducing the virtual load H'_K equal to unity and the virtual moment M'_K equal to unity, the horizontal displacement δ_K and the end rotation θ_K, respectively, can be determined by use of the work equation.

The actual normal force N and bending moment M (Fig. 15(a)) are

$$N = -H_c \cos \phi \quad \ldots\ldots (32)$$

and

$$M = M_K - H_K r_e (\cos \phi - \cos \phi_K) \quad \ldots\ldots (33)$$

Because H'_K is equal to unity (Fig. 15(c)),

$$N' = -\cos \phi \quad \ldots\ldots (34)$$

and

$$M' = -r_e (\cos \phi - \cos \phi_K) \quad \ldots\ldots (35)$$

Hence,

$$\delta_K = \int_{-\phi_K}^{+\phi_K} \frac{M' M \, ds}{E I} + \int_{-\phi_K}^{+\phi_K} \frac{N' N \, ds}{E A} \quad \ldots\ldots (36)$$

Assuming the products $E I$ and $E A$ to be constant, inserting Eqs. 32, 33, 34, and 35 into Eq. 36, and integrating leads to

$$\delta_K \frac{E I}{2 r_e^2} = M_K (\phi_K \cos \phi_K - \sin \phi_K) + H_K r_e \left[\phi_K \left(\tfrac{1}{2} + \cos^2 \phi_K\right) - \tfrac{3}{4} \sin 2 \phi_K + \frac{I}{A r_e^2} \left(\tfrac{1}{2} \phi_K + \tfrac{1}{4} \sin 2 \phi_K\right) \right] \quad \ldots\ldots (37)$$

If M'_K and M' are made equal to unity and N' is made equal to zero, the work equation provides the end rotation θ_K. The reduction of the effective width in the edge-member zone is accounted for by a coefficient of elastic restraint κ. Thus the product of the external moment M'_K equal to unity of the virtual load system times the rotation $(-\kappa M_K)$ caused by the elastic restraint under the actual load system gives a contribution to the external work:

$$\theta_K - \kappa M_K = \int_0^{+\phi_K} \frac{M' M \, ds}{E I} + \int_0^{+\phi_K} \frac{N' N \, ds}{E A} \quad \ldots\ldots (38)$$

Substitution of Eqs. 32 and 33 into Eq. 38 and integrating yields

$$\theta_K \frac{E I}{r_e} = M_K (\phi_K + \tilde{\kappa}) + H_K r_e (\phi_K \cos \phi_K - \sin \phi_K) \quad \ldots\ldots (39)$$

in which

$$\tilde{\kappa} = \frac{E I}{r_e} \kappa \quad \ldots\ldots (40)$$

For any given values of δ_K and θ_K, the two redundants H_K and M_K are determined by Eqs. 37 and 39. The direct stresses in the ribs are determined by use of Eq. 25.

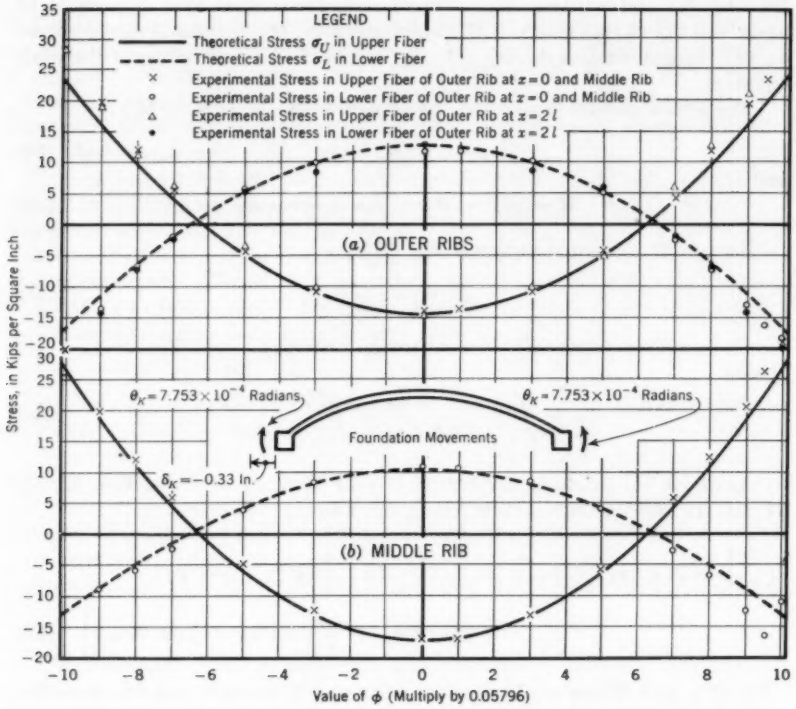

FIG. 16.—THEORETICAL AND EXPERIMENTAL STRESSES IN THE MODEL AS A RESULT OF FOUNDATION MOVEMENTS

Determination of the Shell Forces.—The procedure for determining the shell forces resulting from foundation movements follows the steps used in the case of horizontal longitudinal forces. For the two outer ribs and the middle rib the corresponding F-forces are computed from Eq. 5 following the determination of the stress σ_a along the connecting line of the rib and shell (from Eq. 25). Knowing the boundary conditions for the shell and the F-forces, the stress distribution in the shell can be determined. This analysis can be found elsewhere (14).

Numerical Example.—The model shown in Fig. 1 is analyzed for a given horizontal displacement δ_K and end rotation θ_K. The effective width of the ribs must first be computed. In order to know the number n, used in Fig. 4 to determine the effective width, the stress distribution along the rib must be known. Fig. 16 shows that, as a first approximation, the variation of the stress σ_L in the lower fiber of the middle and outer ribs is a cosine function

with a half-wave length of approximately 0.75 radian. Hence,

$$n = \frac{\pi}{0.75} \cong \frac{3\,\pi}{4\,\phi_K} \ldots\ldots\ldots\ldots\ldots\ldots\ldots\ldots (41)$$

This value of n is a first approximation if symmetrical foundation movements are considered. Inserting the value of ϕ_K (0.5866 radian) into Eq. 41 results in n being equal to 4.14. From Eq. 3, λ is found to equal 0.14. Thus, for the middle rib $\beta\,l$ is equal to 4.42 (greater than 2.4) and for the outer ribs $\beta\,l$ is equal to zero.

From Fig. 4 it is obvious that the values of K for (*a*) $\lambda = 0$, $\beta\,l = \infty$ in case of the middle rib, and (*b*) $\lambda = 0$, $\beta\,l = 0$ in case of the outer ribs are sufficiently accurate for the determination of the effective width. Thus, for the middle rib K is equal to 1.52 in. and b is equal to 5.43 in. For the outer rib K is equal to 0.38 in. and b equals 1.36 in.

The following is a list of values for the effective section of the middle rib.

Item	Value
Area, A	1.961 sq in.
Distance, z_u	−1.382 in.
Distance, z_L	0.731 in.
Distance, z_a	0.672 in.
Radius, r_e	108.731 in.
Moment of inertia, I	0.921 in.^{4}

The ratio of the moment of inertia of the effective section to the moment of inertia of the rib is equal to 1.84. The considerable increase (84%) of the bending stiffness of the middle rib as a result of including the effective width of the shell is especially noteworthy.

On the model a horizontal displacement, δ_K, of 0.3300 in. and an end rotation, ϕ_K, of 7.753×10^{-4} radian were induced.

Assuming for κ the value,

$$\kappa = 0.05\,\frac{r_e}{E\,I} \ldots\ldots\ldots\ldots\ldots\ldots\ldots\ldots (42)$$

and inserting into Eqs. 37 and 39 the proper values, the horizontal thrust H_K and the end moment M_K are determined as follows:

Rib	H_K, in pounds	M_K, in inch-pounds
Middle	−1,636	−17,850
Outer	−946	−10,350

It should be noted that κ depends on the type of loading; for the case of horizontal lateral loads a different value for κ was used.

The normal force N and the bending moment M for an arbitrary angle ϕ along the rib are given by Eqs. 32 and 33. The rib stresses (determined from Eq. 25) are plotted in Fig. 16 for the middle and outer ribs.

Fig. 17 shows the normal force in a circumferential direction N_ϕ and the bending moment in axial direction M_x of the shell.

Experimental Investigation and Comparison.—The same model (Fig. 1), as used for the test of lateral horizontal loads, was subjected to a horizontal

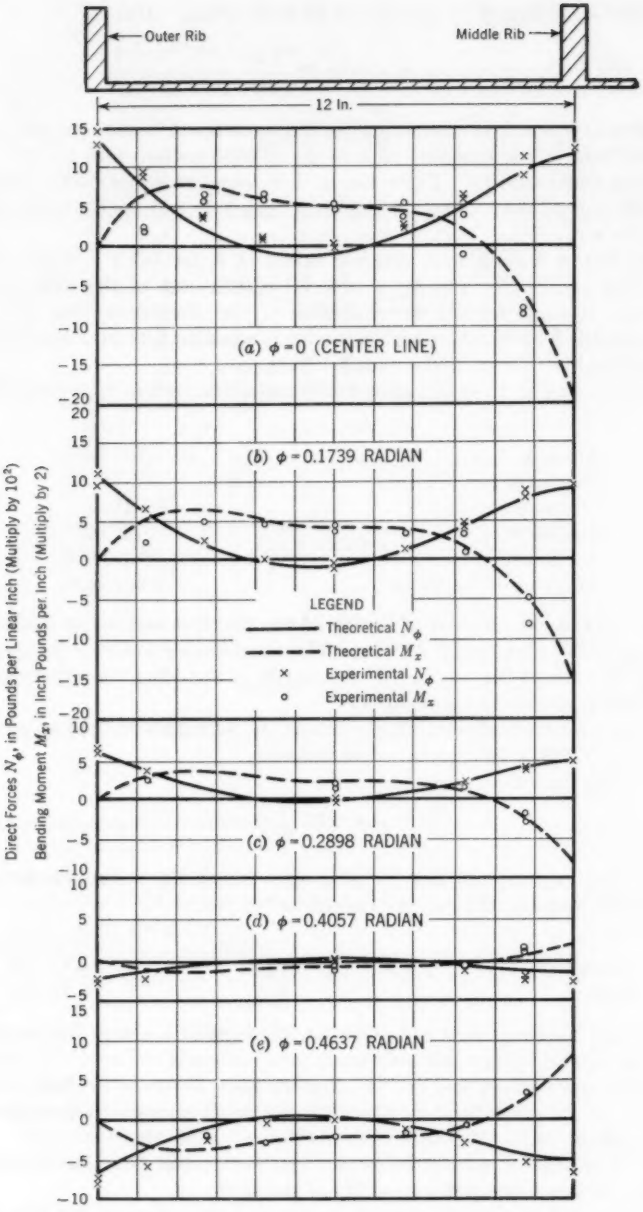

FIG. 17.—NORMAL FORCE IN A CIRCUMFERENTIAL DIRECTION AND BENDING MOMENT IN THE AXIAL DIRECTION

foundation displacement as shown in Fig. 18. The measured displacement and the end rotations are as previously given.

The stresses in the ribs and the N_ϕ-force and M_x-moment computed on the basis of the SR-4 strain-gage readings are plotted in Figs. 16 and 17, respectively. The theoretical analysis and the test results again compare favorably. The discrepancy of a few experimental M_x-values in Fig. 17 does not influence the over-all agreement.

Conclusions Concerning Foundation Movements.—

1. By taking as the effective width of the shell the flange of a T-section (the web of which is the rib), the analysis of the ribs for foundation movements can be accomplished by use of the simple arch theory. Following the determination of the stresses in the ribs, the stress distribution in the shell can also be computed. Experimental results on the model support the theoretical analysis.

2. Eqs. 37 and 39 show that, for given foundation movements δ_K and ϕ_K, the moment M_K and the horizontal thrust H_K are proportional to the moment of inertia I of the effective section of the rib. Neglecting the influence of the normal force on the deformations, which is completely negligible,

$$N = f_1(\phi)\, I \ldots\ldots\ldots\ldots\ldots\ldots\ldots\ldots (43a)$$

and

$$M = f_2(\phi)\, I \ldots\ldots\ldots\ldots\ldots\ldots\ldots\ldots (43b)$$

in which $f_1(\phi)$ and $f_2(\phi)$ are functions of ϕ.

The stress in the rib becomes, from Eq. 25,

$$\sigma = \frac{f_1 I}{A} \pm \frac{f_2 I z}{I} = \frac{f_1 I}{A} \pm f_2 z \ldots\ldots\ldots\ldots\ldots\ldots (44)$$

Thus, σ is approximately proportional to the distance z of the fiber from the centroidal axis of the cross section because the first term of the right side of Eq. 44 is relatively small. The importance of these derivations will be explained subsequently.

Some Special Problems

Uniform Temperature Change and Shrinkage of the Concrete.—Suppose a shell roof undergoes a uniform temperature change of $\Delta t°$. If the whole structure would be supported as a simple beam, this temperature change would cause an increase ΔL of the span L:

$$\Delta L = \alpha\, \Delta t°\, L \ldots\ldots\ldots\ldots\ldots\ldots\ldots\ldots (45)$$

in which α is the coefficient of thermal expansion. Actually this increase (ΔL) is impossible because the abutments are restrained. Therefore the original span L must be restored by diminishing the new span ($L + \Delta L$) by ΔL. The latter is equal to a horizontal displacement, δ_K, previously investigated under the heading, "Foundation Movements." By substituting into Eqs. 37 and 39 the values,

$$\delta_K = \alpha\, \Delta t°\, L \ldots\ldots\ldots\ldots\ldots\ldots\ldots\ldots (46a)$$

and

$$\theta_K = 0 \ldots\ldots\ldots\ldots\ldots\ldots\ldots\ldots\ldots\ldots (46b)$$

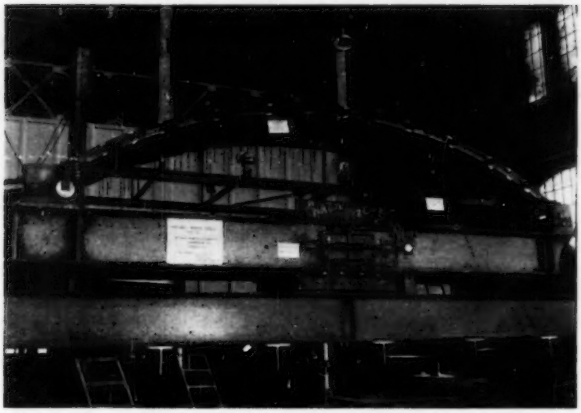

FIG. 18.—LABORATORY MODEL BEING SUBJECTED TO HORIZONTAL FOUNDATION DISPLACEMENT

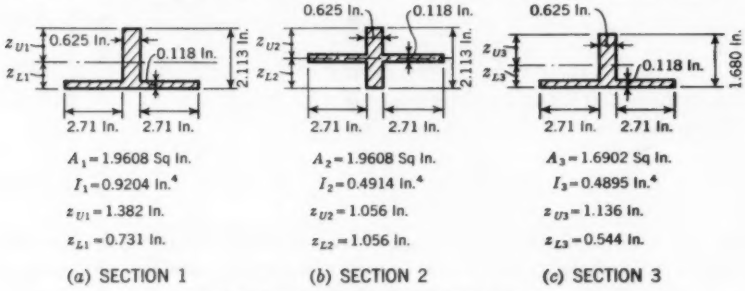

FIG. 19.—VARIATIONS OF THE RIB SECTION

the horizontal thrust H_K and the end moment M_K caused by a temperature rise $\Delta t°$ can be determined.

It is usual to consider the effect of shrinkage of the concrete as equivalent to a fall in temperature of a specified $\Delta t°$. Hence, the stress caused by shrinkage can also be determined by the same procedure.

Differential Temperature Change Between Ribs and Shell.—If there is a temperature difference between the outside and inside air of a shell roof structure, the ribs, exposed mostly to the outside air, will have a different average temperature than the shell. The difference in temperature between the shell and the rib can be considered to be $\Delta t°$. Obviously, stresses will be produced in the structure.

An analysis of this case resulted in thermal stresses as great as 100 lb per sq in. for a temperature difference of 10° F in a hangar of the type built at Rapid City (340-ft span).

The actual temperature distribution will be somewhat different from the assumed one because the temperature will vary continuously. Temperature measurements on an actual structure should be made to determine the variation.

Stability of the Structure.—The thickness t of the shell is mainly governed by stability considerations. For a certain spacing of the ribs, l, a radius r of the shell, and a given distributed load, a minimum thickness t of the shell is required (13) (16). The resulting membrane stresses reach only a fraction of the allowable concrete stresses in compression. It is of interest to note that the ratio of the thickness to the radius of modern shell roofs is smaller than the corresponding ratio for an egg shell. This fact illustrates the perfection to which these structures have been developed.

The ribs, reinforcing the shell at regular intervals l, increase the buckling stiffness of the shell panel. Furthermore, the ribs are indispensable for carrying a one-sided live load (such as snow) acting on the structure. To provide sufficient buckling safety for the entire structure, the ribs must have a specific minimum stiffness. The buckling load is proportional to the moment of inertia of the effective section. Previous considerations concerning the stresses caused by a volume change led to a stiffness of the rib that was as small as possible. Obviously the stiffness should be kept at the minimum required for stability and bending strength so that the stresses caused by a volume change do not become excessive.

Consequently, the factor of safety against buckling of the ribs is important. A smaller factor of safety will require less stiffness, and therefore smaller stresses will be set up by volume changes. Plastic flow of the concrete affects the geometrical shape of the structure, and thus the forces, in a dangerous manner if the factor of safety is decreased excessively. In addition, the secondary moments caused by deformations of the structure can be correlated to the factor of safety against buckling (17) (18).

Location of the Shell with Respect to the Rib.—The idea of placing the shell in the middle of the rib was advocated by C. S. Whitney, M. ASCE, in 1950 (19). Considering the stresses caused by a volume change, Mr. Whitney concluded that the stiffness of the ribs should be a minimum. By placing the shell in the middle of the rib the stiffness of the effective section is diminished to a great extent, as shown in Fig. 19. The same decrease can be obtained, however, by taking a smaller rib, with the shell at one edge of the rib. To illustrate this decrease, the sections shown in Fig. 19 must be considered. Sections 1 and 2 are identical except for the location of the rib. Placing the shell in the middle of the rib reduces the moment of inertia by 47%. Section 3 has a moment of inertia approximately equal to section 2 as a result of the reduction in the height of the rib. The normal force and bending moment caused by the volume changes are proportional to the moment of inertia of the effective section. (Compare Eqs. 37, 39, and 43.) The fiber stresses, however, are approximately proportional to the distance z of the fiber from the neutral axis (Eq. 44). The ratio of the corresponding stresses of the two sections is thus equal to the ratio of the corresponding distances z. Therefore, for the upper fibers,

$$\frac{\sigma_{u3}}{\sigma_{u2}} = \frac{z_{u3}}{z_{u2}} = \frac{1.136}{1.056} = 1.08 \ldots\ldots\ldots\ldots\ldots\ldots (47a)$$

for the lower fiber,

$$\frac{\sigma_{L3}}{\sigma_{L2}} = \frac{z_{L3}}{z_{L2}} = \frac{0.544}{1.056} = 0.52 \ldots\ldots\ldots\ldots\ldots\ldots (47b)$$

Section 3 has in the upper fiber a stress 8% higher and in the lower fiber a stress 48% lower than the stresses in section 2. The objection that in section 3 important cross bending stresses σ_x are set up can be rejected, for in the most extreme case σ_x is 1.73 times the lower fiber stress of the rib (14*b*). Therefore,

$$\frac{\sigma_x}{\sigma_{L2}} = 1.73 \times 0.52 = 0.90 \ldots\ldots\ldots\ldots\ldots\ldots (48)$$

from which it can be seen that the cross bending stress σ_x is 10% smaller than σ_{L2}. Furthermore, the cross bending is concentrated over a very short length.

Therefore, for section 3 with a 21% lighter rib than section 2, the bending moment and normal force caused by volume changes are identical. Neglecting the influence of the normal force, the stresses of section 3 are +8% and −48% of the stresses of section 2. Cross bending stresses σ_x are 10% lower than the maximum stress in section 2 and of local importance. (σ_x has the form of a strongly damped oscillation starting from the rib.) Thus, from theoretical considerations, section 2 does not have any advantage over section 3. Contrarily, 21% of the dead weight of the rib can be saved by using section 3. Therefore, it can be concluded that it is not only ineffective but wasteful to place the shell at the center of the rib.

Conclusions

Theoretical solutions for some problems encountered in designing long-span cylindrical shell roofs were presented. Tests on a steel model in the scale of 1 to 30 of an actual structure built of reinforced concrete (the hangar in Rapid City) confirmed the theoretical analysis. Possible objection to the fact that the test results were obtained from a perfectly elastic model (only elastic strains were induced in the model), whereas the material (reinforced concrete) in the actual structure exhibits quite different properties, can be answered as follows:

It is common practice to compute the forces and moments in statically indeterminate concrete structures by assuming the concrete to be a perfectly elastic material. The moment of inertia for a cross section is taken for the uncracked concrete section. On the basis of the computed moments and normal forces, the stresses in the concrete and the reinforcing steel are determined under the assumption that the concrete is ineffective in tension. This can be done by using either the "*n*-theory" or the "limit-design theory."

Therefore, the similitude between the theoretical direct forces and the bending moment in the steel model and the concrete structure can be made. These values were checked by results of the tests performed on the model, built of a nearly perfectly elastic material. Between the stresses in the model and in the actual structure no such direct relationships can be derived. It is an established fact (proved by many tests), however, that reinforced concrete structures, analyzed as elastic structures and reinforced according to the computed moments and normal forces, behave essentially as predicted.

Many tests, not reported herein, were made during the course of the investigation. Similar procedures of analysis, based on the use of the effective width, were found to be adequate in checking test results to a close approximation in all cases.

It was found satisfactory to estimate roughly the value of n, since the

effective width for the proportions of structures tested and the type of stress variation induced by usual loads put n in a region where variations caused little or no change in the effective width. Other engineering uncertainties are of much greater magnitude. In applying this analysis to different problems, it may be necessary to perform analyses by use of a Fourier series representation of the stress variation along the juncture of the rib and shell. In such cases effective widths and stresses could be determined for each of the significant terms of the Fourier series, and the actual stress at any point could be determined by superposition.

Acknowledgments

This paper presents the results of part of the theoretical and experimental studies made during the course of a two-year research program on shell arch roofs performed at the Fritz Engineering Laboratory. K. R. Harpel, foreman of the laboratory, gave valuable assistance throughout the experimental investigation.

The Roberts and Schaefer Company of Chicago, Ill., was the sponsor of the research program. Thanks are extended to J. E. Kalinka, Robert Zaborowski, A. M. ASCE, Anton Tedesko, M. ASCE, Otto Gruenwald, W. A. Renner, A. M. ASCE, and Paul Rongved, M. ASCE—all of the Roberts and Schaefer Company.

APPENDIX I. NOTATION

The following symbols adopted for use in the paper and for the guidance of discussers, conform essentially with "American Standard Symbols for Structural Analysis" (ASA-Z 10.8–1949), prepared by a committee of the American Standards Association with Society representation, and approved by the Association in 1949:

A = cross-sectional area;
b = effective width of the shell;
E = modulus of elasticity;
F = total direct force defined in Eq. 5;
H_c = horizontal thrust at the center of a rib shown in Fig. 8(*a*);
H_K = horizontal thrust on rib shown in Fig. 15(*a*);
H'_K = virtual horizontal thrust;
I = moment of inertia;
I_c = moment of inertia at the center of a rib;
K = a function of λ and βl, graphically represented in Fig. 4;
L = span of the roof;
l = overhang distance;
M = total bending moment:
M' = virtual bending moment;
M_B = bending moment on a unit;
M_c = bending moment at the center of a rib shown in Fig. 8(*a*);
M_K = restraining moment;
M'_K = virtual restraining moment;
M_o = bending moment of rib in statically determinate system;
M_T = twisting moment;

N = total normal force:
- N' = virtual normal force;
- N_o = normal force of rib in statically determinate system;
- N_x = direct force per unit width of shell in the axial direction;
- N_ϕ = direct force per unit width of shell in the circumferential direction;
- $N_{\phi x}$ and $N_{x\phi}$ = direct shear forces per unit width of shell in circumferential and axial direction, respectively;

n = number of complete waves made by a harmonic function around the circumference of a cylinder;
P' = virtual load;
p = applied uniformly distributed load;
r = radius of the cylinder;
r_c = radius of the effective rib section;
s = distance;
V = shear force on a unit;
x = coordinate in axial direction of shell;
z = distance of a fiber from the centroidal axis of the effective section;
z_a = distance from the loads $N_{\phi x}$ to the centroid of the effective section;
α = coefficient of thermal expansion;
β = shell constant defined in Eq. 4;
δ_K = known horizontal movement;
θ_K = known rotation of the abutment;
- θ_{Kl} = rotation of the left abutment;
- θ_{Kr} = rotation of the right abutment;

κ = coefficient of elastic restraint;
λ = parameter defined by Eq. 3;
σ_a = circumferential stress along the connecting line of rib and shell;
- σ_L = circumferential stress in the lower fiber;
- σ_x = cross bending stress;

$\tau_{\phi x}$ and $\tau_{x\phi}$ = shearing stresses;
ϕ = angle defined in Figs. 5 and 8;
ϕ_K = angle defined in Figs. 5 and 8; and
ω = angle defined in Fig. 8(*b*).

APPENDIX II. BIBLIOGRAPHY

(1) **"Elasticity,"** by A. E. H. Love, Cambridge University Press, Cambridge, England, 4th Ed., 1927.

(2) **"Da : Elastizitätsproblem für dünne Schalen,"** by E. Meissner, *Physikalische Zeitschrift*, Vol. 14, 1913, p. 343.

(3) **"Ueber Elastizität und Festigkeit dünner Schalen,"** by E. Meissner, *Vierteljahrsschrift*, Naturforschenden Gesellschaft, Zürich, Switzerland, Vol. 60, 1915, p. 23.

(4) **"Handbuch für Eisenbeton-Bau,"** Wilhelm Ernst und Sohn, Vol. VI, 4th Ed., 1928, p. 269.

(5) **"Die querversteiften zylindrischen Schalengewölbe mit kreissegmentförmigem Querschnitt,"** by U. Finsterwalder, *Ingenieur Archiv*, Vol. 4, 1933, p. 43.

(6) **"Die strenge Theorie der Kreiszylinderschale und ihre Anwendung auf die Z. D. Schalen,"** by F. Dischinger, *Beton und Eisen*, Vol. 34, 1935.

(7) **"Principles of Concrete Shell Dome Design,"** by E. C. Molke and J. E. Kalinka, *Proceedings*, A. C. I., Vol. 9, 1938, p. 649.

(8) **"Thin Concrete Arch Roof Provides 340 Ft. Clear Span For Bomber Hangar,"** by L. W. Prentiss, *Civil Engineering*, Vol. 19, 1949, p. 86. (*a*) p. 87.

(9) **"Construction of Long-Span Concrete Arch Hangar at Limestone Air Force Base,"** by J. E. Allen, *Proceedings*, A. C. I., Vol. 21, 1950, p. 405.

(10) **"The Effective Width of a Circular Cylindrical Shell Adjacent to a Circumferential Reinforcing Rib,"** by B. Thürlimann, R. Bereuter, and B. G. Johnston, *Proceedings*, The First National Cong. for Applied Mechanics, published by the ASME, 1952, p. 347.

(11) **"Die mittragende Breite,"** by T. von Kármàn, *Festschrift August Föppls*, J. Springer Verlag, Berlin, Germany, 1924, p. 114.

(12) **"The Determination of the Effective Width of Wide-Flanged Beams,"** by W. Raithel, *Technical Report No. 61*, Ordnance Research and Development Div., U. S. Dept. of Army, Washington, D. C., 1949.

(13) **"Theory of Plates and Shells,"** by S. Timoshenko, McGraw-Hill Book Co., Inc., New York, N. Y., 1940, p. 433. (*a*) p. 392.

(14) **"The Effective Width of Circular Cylindrical Shells Reinforced by Ribs,"** by B. Thürlimann, dissertation presented to Lehigh Univ., at Bethlehem, Pa., in partial fulfillment of the requirements for the degree of Doctor of Philosophy, 1950, (*a*) p. 25. (*b*) p. 42.

(15) **"The Effective Width of Cylinders Periodically Stiffened by Circular Rings,"** by C. B. Biezeno and J. J. Koch, *Proceedings*, Koninklijke Nederlandsche Academie, Van Weten-Schappen, Vol. XLVIII, 1945, p. 147.

(16) **"Statik und Dynamik der Schalen,"** by W. Flügge, J. Springer Verlag, Berlin, Germany, 1934, p. 112.

(17) **"Untersuchungen über die Knicksicherheit,"** by F. Dischinger, *Bau-Ingenieur*, Vol. 18, 1937, p. 487.

(18) **"Elastische und plastische Verformungen,"** by F. Dischinger, *ibid.*, Vol. 20, 1939, p. 53.

(19) **"Cost of Long-Span Concrete Shell Roofs,"** by C. S. Whitney, *Proceedings*, A. C. I., Vol. 21, 1950, p. 765.

AMERICAN SOCIETY OF CIVIL ENGINEERS

OFFICERS FOR 1954

PRESIDENT

DANIEL VOIERS TERRELL

VICE-PRESIDENTS

Term expires October, 1954:
EDMUND FRIEDMAN
G. BROOKS EARNEST

Term expires October, 1955:
ENOCH R. NEEDLES
MASON G. LOCKWOOD

DIRECTORS

Term expires October, 1954:
WALTER D. BINGER
FRANK A. MARSTON
GEORGE W. McALPIN
JAMES A. HIGGS
I. C. STEELE
WARREN W. PARKS

Term expires October, 1955:
CHARLES B. MOLINEAUX
MERCEL J. SHELTON
A. A. K. BOOTH
CARL G. PAULSEN
LLOYD D. KNAPP
GLENN W. HOLCOMB
FRANCIS M. DAWSON

Term expires October, 1956:
WILLIAM S. LaLONDE, JR.
OLIVER W. HARTWELL
THOMAS C. SHEDD
SAMUEL B. MORRIS
ERNEST W. CARLTON
RAYMOND F. DAWSON

PAST-PRESIDENTS

Members of the Board

CARLTON S. PROCTOR
WALTER L. HUBER

TREASURER

CHARLES E. TROUT

EXECUTIVE SECRETARY

WILLIAM N. CAREY

ASSISTANT TREASURER

GEORGE W. BURPEE

ASSISTANT SECRETARY

E. L. CHANDLER

PROCEEDINGS OF THE SOCIETY

HAROLD T. LARSEN
Manager of Technical Publications

DEFOREST A. MATTESON, JR.
Editor of Technical Publications

PAUL A. PARISI
Assoc. Editor of Technical Publications

COMMITTEE ON PUBLICATIONS

FRANK A. MARSTON, *Chairman*

I. C. STEELE
GLENN W. HOLCOMB
ERNEST W. CARLTON
OLIVER W. HARTWELL
SAMUEL B. MORRIS